

# A fully “locking-free” isogeometric approach for plane linear elasticity problems: a stream function formulation

F. Auricchio<sup>a,b</sup>, L. Beirão da Veiga<sup>d</sup>, A. Buffa<sup>b</sup>,  
C. Lovadina<sup>c,b,1</sup>, A. Reali<sup>a</sup>, and G. Sangalli<sup>c,b</sup>

<sup>a</sup> *Dipartimento di Meccanica Strutturale, Università di Pavia, Italy*

<sup>b</sup> *IMATI-CNR, Pavia, Italy*

<sup>c</sup> *Dipartimento di Matematica, Università di Pavia, Italy*

<sup>d</sup> *Dipartimento di Matematica, Università di Milano, Italy*

---

## Abstract

In this paper, we study plane incompressible elastic problems by means of a “stream-function” formulation such that a *divergence-free* displacement field can be computed from a scalar potential. The numerical scheme is constructed within the framework of NURBS-based isogeometric analysis and we take advantage of the high continuity guaranteed by NURBS basis functions in order to obtain the displacement field from the potential differentiation. As a consequence, the obtained numerical scheme is automatically locking-free in the presence of the incompressibility constraint. A Discontinuous Galerkin approach is proposed to deal with multiple mapped, possibly multiply connected, domains. Extensive numerical results are provided to show the method capabilities.

*Key words:* incompressible elasticity, stream function formulation, isogeometric analysis, NURBS.

---

---

<sup>1</sup> Corresponding author.

Address: Dipartimento di Matematica, Università di Pavia.

Via Ferrata 1, I-27100, Italy.

Tel.: ++39-0382-985685. Fax: ++39-0382-985602

E-mail: carlo.lovadina@unipv.it

## Introduction

In this work we focus on two-dimensional plane strain linear elastic problems and we investigate the possibility of solving in an exact way the constraint induced by the incompressibility condition through the use of an *isogeometric interpolation* based on Non-Uniform Rational B-Splines (NURBS), see [15]. In particular, we take advantage of the fact that high continuity across the elements is easily achieved by NURBS functions.

It is well known that it is possible to rewrite the incompressible elastic problem as an *elliptic fourth order* problem in terms of a scalar potential (referred to as *stream function*, see [12]) whose **curl** gives the displacement field. That is, the problem is rewritten such to have only a single scalar field unknown (implying less degrees of freedom than the original problem) and the displacements are obtained computing the **curl** of such a scalar field in post-processing. The obtained solution is divergence-free by construction and, hence, the incompressibility constraint is automatically and exactly satisfied.

The trade-off of this methodology is the need to construct a solution characterized by higher continuity than the one required by the original problem. This aspect represents a severe drawback for standard numerical techniques such as finite elements, because rather complicated methods must be adopted (see, for instance, the elements detailed in [2]). In the present paper this difficulty is perfectly circumvented and solved resorting to isogeometric analysis [15], which may be seen as a generalization of classical finite element analysis. Indeed, the NURBS-based isogeometric approach allows to use shape functions smoother than the standard  $C^0$ -continuity of finite elements. Another strength of that approach, which is of great relevance in all engineering applications, is that it makes possible the exact geometric representation of CAD objects and simplifies mesh refinement (see [15]).

Accordingly, combining the stream function reformulation and the NURBS-based technique we end up with a discretization procedure for which volumetric locking effects cannot occur. Therefore, the proposed formulation represents a highly accurate alternative to more classical approaches, such as mixed or enhanced strain finite element methods (see [9] or [21], for instance).

The paper starts with a presentation of the stream function formulation for plane linear elasticity. Then, after a brief review of some basic concepts of Non-Uniform Rational B-Splines (NURBS), we introduce the isogeometric approach that is employed both for describing the problem geometry and for approximating the stream function. Moreover, we sketch an extension of our formulation to deal with 3D problems. We also outline a Discontinuous Galerkin type approach to deal with the case of multi-patch domains, thus

including multiply connected geometries. Finally, we present extensive numerical tests in order to show the capabilities of the method on some significant model problems. In particular, a first comparison with some mixed-enhanced finite elements (see [5,16]) shows a superior behaviour of our NURBS-based discretization. As a conclusion, future directions of research on the proposed formulation are drawn.

## 1 The plane linear elasticity problem for incompressible materials

We consider the plane linear elasticity problem in the framework of the infinitesimal theory (cf., e.g. [14] or [20]) for a homogeneous isotropic incompressible material. The elastic body occupies a regular region  $\Omega$  in  $\mathbb{R}^2$  with boundary  $\partial\Omega = \overline{\Gamma_D \cup \Gamma_N}$  such that  $\Gamma_D \cap \Gamma_N = \emptyset$ . We are therefore led to solve the following boundary-value problem:

$$\left\{ \begin{array}{ll} \text{Find } (\mathbf{u}, \pi) \text{ such that} & \\ - \mathbf{div} (2\mu\boldsymbol{\varepsilon}(\mathbf{u}) + \pi\boldsymbol{\delta}) = \mathbf{f} & \text{in } \Omega \\ \mathbf{div} \mathbf{u} = 0 & \text{in } \Omega \\ \mathbf{u} = \mathbf{0} & \text{on } \Gamma_D \\ (2\mu\boldsymbol{\varepsilon}(\mathbf{u}) + \pi\boldsymbol{\delta}) \cdot \mathbf{n} = \mathbf{g} & \text{on } \Gamma_N \end{array} \right. \quad (1)$$

where  $\mathbf{u} = (u_1, u_2), \Omega \rightarrow \mathbb{R}^2$  is the displacement field,  $\pi, \Omega \rightarrow \mathbb{R}$  is the pressure-like field,  $\mathbf{f} = (f_1, f_2), \Omega \rightarrow \mathbb{R}^2$  and  $\mathbf{g} = (g_1, g_2), \Gamma_N \rightarrow \mathbb{R}^2$  are loading terms. Moreover,  $\boldsymbol{\varepsilon}(\cdot)$  is the usual symmetric gradient operator acting on vector fields, while  $\boldsymbol{\delta}$  is the second-order identity tensor. Finally,  $\mu$  is the Lamé coefficient, for which we suppose that  $0 < \mu_0 \leq \mu \leq \mu_1 < +\infty$ .

Let  $H_D^1(\Omega)$  be the Sobolev space of  $H^1$  functions vanishing on  $\Gamma_D$ . We recall that a standard variational formulation of problem (1) consists in finding  $(\mathbf{u}, \pi) \in \mathbf{V} \times Q = (H_D^1(\Omega))^2 \times L^2(\Omega)$  which solves the system:

$$\left\{ \begin{array}{ll} 2\mu \int_{\Omega} \boldsymbol{\varepsilon}(\mathbf{u}) : \boldsymbol{\varepsilon}(\mathbf{v}) + \int_{\Omega} \pi \operatorname{div} \mathbf{v} = \int_{\Omega} \mathbf{f} \cdot \mathbf{v} + \int_{\Gamma_N} \mathbf{g} \cdot \mathbf{v} & \forall \mathbf{v} \in \mathbf{V} \\ \int_{\Omega} q \operatorname{div} \mathbf{u} = 0 & \forall q \in Q . \end{array} \right. \quad (2)$$

If  $\Gamma_D = \partial\Omega$ , one has to set  $Q = L^2(\Omega)/\mathbb{R}$ .

It is well-known that problem (2) is well-posed and it fits into the theory extensively studied in [9], for instance. However, its finite element discretization

requires some care in order to overcome the *volumetric locking phenomenon*. A detailed discussion on this issue can be found in [9], for example.

In this paper, we will not consider numerical strategies based on formulation (2). Instead, we introduce the space of *divergence-free* functions:

$$\mathbf{K} = \{\mathbf{v} \in \mathbf{V}, \operatorname{div} \mathbf{v} = 0\} \subset \mathbf{V}, \quad (3)$$

and we notice that the displacement field  $\mathbf{u} \in \mathbf{V}$ , part of the solution of system (2), is determined by solving the variational equation:

$$\left\{ \begin{array}{l} \text{Find } \mathbf{u} \in \mathbf{K} \text{ such that} \\ 2\mu \int_{\Omega} \boldsymbol{\varepsilon}(\mathbf{u}) : \boldsymbol{\varepsilon}(\mathbf{v}) = \int_{\Omega} \mathbf{f} \cdot \mathbf{v} + \int_{\Gamma_N} \mathbf{g} \cdot \mathbf{v} \quad \forall \mathbf{v} \in \mathbf{K}. \end{array} \right. \quad (4)$$

Assume now that  $\Omega$  is a simply connected domain. Then, given  $\mathbf{v} \in \mathbf{K}$ , there exists a *uniquely defined* scalar potential  $\varphi \in H^2(\Omega)/\mathbb{R}$  such that:

$$\mathbf{v} = \mathbf{curl} \varphi, \quad (5)$$

where  $\mathbf{curl} = (\partial/\partial y, -\partial/\partial x)$ , see [12]. Setting:

$$\Phi = \{\varphi \in H^2(\Omega)/\mathbb{R}, \mathbf{curl} \varphi = \mathbf{0} \text{ on } \Gamma_D\}, \quad (6)$$

it is easily seen that  $\mathbf{curl}$  provides an (algebraic and topological) isomorphism between  $\Phi$  and  $\mathbf{K}$ . As a consequence, we can write the solution  $\mathbf{u}$  of (4) as  $\mathbf{u} = \mathbf{curl} \psi$ , where  $\psi \in \Phi$  is the solution of the following problem:

$$\left\{ \begin{array}{l} \text{Find } \psi \in \Phi \text{ such that} \\ 2\mu \int_{\Omega} \boldsymbol{\varepsilon}(\mathbf{curl} \psi) : \boldsymbol{\varepsilon}(\mathbf{curl} \varphi) = \int_{\Omega} \mathbf{f} \cdot \mathbf{curl} \varphi + \int_{\Gamma_N} \mathbf{g} \cdot \mathbf{curl} \varphi \quad \forall \varphi \in \Phi. \end{array} \right. \quad (7)$$

Observe that (7) is the usual stream-function formulation for the Stokes problem (see [12]): it will be the basis for the discretization technique we will propose in Section 2.3. Notice also that (7) is a fourth order elliptic (symmetric) problem.

## 2 The NURBS-Based Isogeometric Analysis

In this section, we first present a brief summary of NURBS-based Isogeometric Analysis for two-dimensional problems, for which an extensive account has been given in [6,10,15]. We then introduce our numerical strategy for the stream function formulation (7).

We recall that Non-Uniform Rational B-Splines (NURBS) are a standard tool for describing and modeling curves, surfaces and solids in computer aided design (CAD) and computer graphics (see [17] and [18]). A short description of these functions follows.

### 2.1 B-Splines and NURBS

B-splines in the plane are piecewise polynomial curves composed of linear combinations of B-spline basis functions. The coefficients are points in the plane, referred to as *control points*.

A *knot vector* is a set of non-decreasing real numbers representing coordinates in the parametric space of the curve:

$$\{\xi_1 = 0, \dots, \xi_{n+p+1} = 1\}, \quad (8)$$

where  $p$  is the order of the B-spline and  $n$  is the number of basis functions (and control points) necessary to describe it. A knot vector is said to be *uniform* if its knots are uniformly-spaced and *non-uniform* otherwise. Moreover, a knot vector is said to be *open* if its first and last knots are repeated  $p + 1$  times. In what follows, we always employ open knot vectors. Basis functions formed from open knot vectors are interpolatory at the ends of the parametric interval  $[0, 1]$  but are not, in general, interpolatory at interior knots.

Given a knot vector, univariate B-spline basis functions are defined recursively starting with  $p = 0$  (piecewise constants):

$$N_{i,0}(\xi) = \begin{cases} 1 & \text{if } \xi_i \leq \xi < \xi_{i+1} \\ 0 & \text{otherwise.} \end{cases} \quad (9)$$

For  $p > 1$  :

$$N_{i,p}(\xi) = \frac{\xi - \xi_i}{\xi_{i+p} - \xi_i} N_{i,p-1}(\xi) + \frac{\xi_{i+p+1} - \xi}{\xi_{i+p+1} - \xi_{i+1}} N_{i+1,p-1}(\xi). \quad (10)$$

In Figure 1 we present an example consisting of  $n = 9$  cubic basis functions

generated from the open knot vector  $\{0, 0, 0, 0, 1/6, 1/3, 1/2, 2/3, 5/6, 1, 1, 1, 1\}$ .

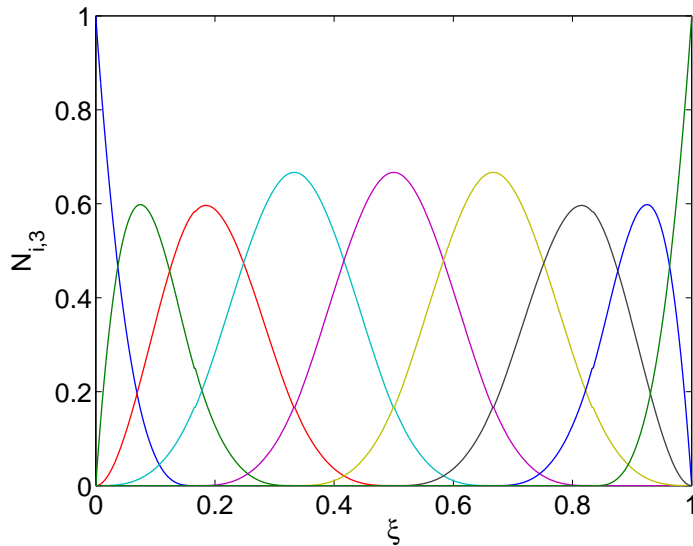


Fig. 1. Cubic basis functions formed from the open knot vector  $\{0, 0, 0, 0, 1/6, 1/3, 1/2, 2/3, 5/6, 1, 1, 1, 1\}$ .

An important property of B-spline basis functions is that they are  $C^{p-1}$ -continuous, if internal knots are not repeated. If a knot has multiplicity  $k$ , the basis is  $C^{p-k}$ -continuous at that knot. In particular, when a knot has multiplicity  $p$ , the basis is  $C^0$  and interpolatory at that location.

By means of tensor products, a B-spline region can be constructed starting from knot vectors  $\{\xi_1 = 0, \dots, \xi_{n+p+1} = 1\}$  and  $\{\eta_1 = 0, \dots, \eta_{m+q+1} = 1\}$ , and an  $n \times m$  net of control points  $\mathbf{B}_{i,j}$ . Two-dimensional basis functions  $N_{i,p}$  and  $M_{j,q}$  (with  $i = 1, \dots, n$  and  $j = 1, \dots, m$ ) of order  $p$  and  $q$ , respectively, are defined from the knot vectors, and the B-spline region is the image of the map  $\mathbf{S} : [0, 1] \times [0, 1] \rightarrow \bar{\Omega}$  given by:

$$\mathbf{S}(\xi, \eta) = \sum_{i=1}^n \sum_{j=1}^m N_{i,p}(\xi) M_{j,q}(\eta) \mathbf{B}_{i,j}. \quad (11)$$

The two-dimensional parametric space is the domain  $[0, 1] \times [0, 1]$ . Observe that the two knot vectors  $\{\xi_1 = 0, \dots, \xi_{n+p+1} = 1\}$  and  $\{\eta_1 = 0, \dots, \eta_{m+q+1} = 1\}$  generate in a natural way a mesh of rectangular elements in the parametric space.

A rational B-spline in  $\mathbb{R}^2$  is the projection onto two-dimensional physical space of a polynomial B-spline defined in three-dimensional homogeneous coordinate space. For a complete discussion of these space projections, see [11] and references therein. In this way, a great variety of geometrical entities can be

constructed and, in particular, all conic sections can be obtained exactly. The projective transformation of a B-spline curve yields a rational polynomial curve. Note that when we refer to the “order” of a NURBS curve, we mean the order of the polynomial curve from which the rational curve was generated.

To obtain a NURBS curve in  $\mathbb{R}^2$ , we start from a set  $\mathbf{B}_i^w$  ( $i = 1, \dots, n$ ) of control points (“projective points”) for a B-spline curve in  $\mathbb{R}^3$  with knot vector  $\Xi$ . Then the control points for the NURBS curve are:

$$(\mathbf{B}_i)_j = \frac{(\mathbf{B}_i^w)_j}{w_i}, \quad j = 1, 2 \quad (12)$$

where  $(\mathbf{B}_i)_j$  is the  $j^{\text{th}}$  component of the vector  $\mathbf{B}_i$  and  $w_i = (\mathbf{B}_i^w)_3$  is referred to as the  $i^{\text{th}}$  *weight*. The NURBS basis functions of order  $p$  are then defined as:

$$R_i^p(\xi) = \frac{N_{i,p}(\xi)w_i}{\sum_{\hat{i}=1}^n N_{\hat{i},p}(\xi)w_{\hat{i}}}. \quad (13)$$

The NURBS curve is defined by:

$$\mathbf{C}(\xi) = \sum_{i=1}^n R_i^p(\xi)\mathbf{B}_i. \quad (14)$$

Analogously to B-splines, NURBS basis functions on the two-dimensional parametric space  $[0, 1] \times [0, 1]$  are defined as:

$$R_{i,j}^{p,q}(\xi, \eta) = \frac{N_{i,p}(\xi)M_{j,q}(\eta)w_{i,j}}{\sum_{\hat{i}=1}^n \sum_{\hat{j}=1}^m N_{\hat{i},p}(\xi)M_{\hat{j},q}(\eta)w_{\hat{i},\hat{j}}}, \quad (15)$$

where  $w_{i,j} = (\mathbf{B}_{i,j}^w)_3$ . Observe that the continuity and supports of NURBS basis functions are the same as for B-splines.

NURBS regions, similarly to B-spline regions, are defined in terms of the basis functions (15). In particular we assume from now on that the physical domain  $\Omega$  is a NURBS region associated with the  $n \times m$  net of control points  $\mathbf{B}_{i,j}$ , and we introduce the geometrical map  $\mathbf{F} : [0, 1] \times [0, 1] \rightarrow \bar{\Omega}$  given by:

$$\mathbf{F}(\xi, \eta) = \sum_{i=1}^n \sum_{j=1}^m R_{i,j}^{p,q}(\xi, \eta)\mathbf{B}_{i,j}. \quad (16)$$

## 2.2 Isogeometric Analysis

The image of the elements in the parametric spaces are elements in the physical spaces. The physical mesh is therefore:

$$\mathcal{T}_h = \{\mathbf{F}((\xi_i, \xi_{i+1}) \times (\eta_j, \eta_{j+1})), \text{ with } i = 1, \dots, n + p, j = 1, \dots, m + q\}. \quad (17)$$

We denote by  $h$  the mesh-size, that is, the maximum diameter of the elements of  $\mathcal{T}_h$ .

Following the isoparametric approach, the space of NURBS functions on  $\Omega$  is defined as the span of the *push-forward* of the basis functions (15):

$$\mathcal{V}_h = \text{span}\{R_{i,j}^{p,q} \circ \mathbf{F}^{-1}\}_{i=1,\dots,n;j=1,\dots,m}. \quad (18)$$

## 2.3 Numerical method

We introduce here the NURBS conforming discretization of the variational problem (7). Let  $\mathcal{V}_h$  denote a NURBS space as introduced in (18), of regularity  $C^k$ ,  $k \geq 1$ , and degree  $p > k$ . We have  $\mathcal{V}_h \subset H^2(\Omega)$ , and then we can introduce the following conforming discretizations of  $\Phi$ :

$$\Phi_h = \mathcal{V}_h \cap \Phi. \quad (19)$$

The numerical method for (7) we propose is a plain Galerkin formulation: the approximated displacement is defined as  $\mathbf{u}_h = \mathbf{curl} \psi_h$ , where  $\psi_h \in \Phi_h$  is the solution of the problem:

$$\left\{ \begin{array}{l} \text{Find } \psi_h \in \Phi_h \text{ such that} \\ 2\mu \int_{\Omega} \boldsymbol{\varepsilon}(\mathbf{curl} \psi_h) : \boldsymbol{\varepsilon}(\mathbf{curl} \varphi_h) = \int_{\Omega} \mathbf{f} \cdot \mathbf{curl} \varphi_h + \int_{\Gamma_N} \mathbf{g} \cdot \mathbf{curl} \varphi_h \quad \forall \varphi_h \in \Phi_h. \end{array} \right. \quad (20)$$

Observe that (20) is uniformly coercive and continuous, hence well-posed.

## 3 A brief discussion on possible extensions

In this Section we briefly sketch some possible extensions of formulation (20) to more complicated case. A complete analysis of such situations is beyond the aims of the present paper, and will be provided in future works.

### 3.1 Three dimensional case

Our formulation (7) relies on the existence of a *scalar* potential  $\varphi$  for a divergence free field  $\mathbf{v}$  such that (5) holds true. It is well known that in  $3D$ , even for simply connected domains, the representation (5) does not hold, but instead each divergence free field can be represented in terms of a *vector* potential  $\boldsymbol{\varphi}$  such that  $\mathbf{v} = \mathbf{curl} \boldsymbol{\varphi}$ . Moreover, the vector potential  $\boldsymbol{\varphi}$  is not unique and it is determined up to a gradient of a function in  $H^1(\Omega)$ . This implies that if we use formulation (7) in three dimension verbatim, we will not obtain a well-posed problem due to the lack of solution uniqueness. We propose here a possible modification of (7) which does not change the nature of the formulation, thus showing that it is possible to tackle  $3D$  problems as well. In what follows, for the sake of exposition, we suppose for simplicity that  $\Omega$  is a simply connected Lipschitz bounded domain in  $\mathbb{R}^3$  with connected boundary  $\partial\Omega$ .

Following [1, Equation (3.36)], the vector potential  $\boldsymbol{\varphi}$  is uniquely determined if

$$\begin{aligned} \mathbf{v} &= \mathbf{curl} \boldsymbol{\varphi} & \operatorname{div} \boldsymbol{\varphi} &= 0 & \text{in } \Omega, \\ \boldsymbol{\varphi} \cdot \mathbf{n} &= 0 & & & \text{on } \partial\Omega. \end{aligned} \quad (21)$$

This suggests how to extend formulation (7) in  $3D$ . Let

$$\begin{aligned} \boldsymbol{\Phi} = \{ \boldsymbol{\varphi} \in L^2(\Omega)^3, \operatorname{div} \boldsymbol{\varphi} \in H^1(\Omega)^3, \mathbf{curl} \boldsymbol{\varphi} \in H^1(\Omega)^3, \\ \boldsymbol{\varphi} \cdot \mathbf{n} = 0 \text{ on } \partial\Omega, \mathbf{curl} \boldsymbol{\varphi} = 0 \text{ on } \Gamma_D \}. \end{aligned} \quad (22)$$

Regularity issues concerning vector fields in  $\boldsymbol{\Phi}$  are addressed in [1]. Following again [1], and using Poincaré-Friedrichs inequality,  $\boldsymbol{\Phi}$  is a Hilbert space endowed with the norm ( $\Gamma_D \neq \emptyset$ ):

$$\|\boldsymbol{\varphi}\|_{\boldsymbol{\Phi}}^2 := |\mathbf{curl} \boldsymbol{\varphi}|_{1,\Omega}^2 + |\operatorname{div} \boldsymbol{\varphi}|_{1,\Omega}^2 \quad (23)$$

where  $|\cdot|_{1,\Omega}$  denotes the  $H^1$ -seminorm. Problem (7) can be reformulated in  $3D$  as follows:

$$\begin{cases} \text{Find } \boldsymbol{\psi} \in \boldsymbol{\Phi} \text{ such that} \\ a(\boldsymbol{\psi}, \boldsymbol{\varphi}) = \int_{\Omega} \mathbf{f} \cdot \mathbf{curl} \boldsymbol{\varphi} + \int_{\Gamma_N} \mathbf{g} \cdot \mathbf{curl} \boldsymbol{\varphi} & \forall \boldsymbol{\varphi} \in \boldsymbol{\Phi}, \end{cases} \quad (24)$$

where

$$a(\boldsymbol{\psi}, \boldsymbol{\varphi}) = 2\mu \int_{\Omega} \boldsymbol{\varepsilon}(\mathbf{curl} \boldsymbol{\psi}) : \boldsymbol{\varepsilon}(\mathbf{curl} \boldsymbol{\varphi}) + 2\mu \int_{\Omega} \nabla \operatorname{div} \boldsymbol{\psi} \cdot \nabla \operatorname{div} \boldsymbol{\varphi}. \quad (25)$$

Korn's inequality ensures coercivity of the bilinear form  $a(\cdot, \cdot)$  in the  $\|\cdot\|_{\boldsymbol{\Phi}}$  norm (as soon as  $\Gamma_D \neq \emptyset$ ), thus the solution uniqueness is guaranteed. Finally, it is

easy to check that  $\mathbf{curl} \boldsymbol{\psi}$  is the solution of the elasticity problem. Therefore, we may discretize problem (24) using the NURBS approximation, as described in Section 2.

### 3.2 Multipatch formulation

We consider the case where the domain  $\Omega$  needs to be split into  $N$  patches  $\Omega_\alpha$ ,  $\alpha = 1, \dots, N$ , described by  $N$  different geometrical maps

$$\mathbf{F}_\alpha : [0, 1] \times [0, 1] \rightarrow \bar{\Omega}_\alpha \quad \alpha = 1, \dots, N.$$

This occurs in the description of complex and/or multiply connected geometries, as depicted in Figures 2–3 (note that each patch is topologically equivalent to the parametric domain  $[0, 1] \times [0, 1]$ ).

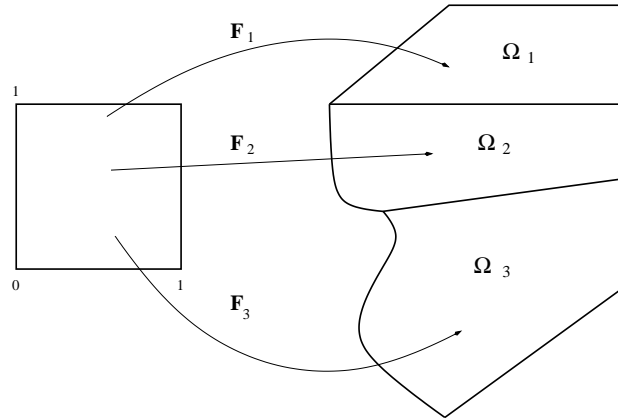


Fig. 2. Simply connected  $\Omega$ , split into three domains  $\Omega_1$ ,  $\Omega_2$  and  $\Omega_3$ .

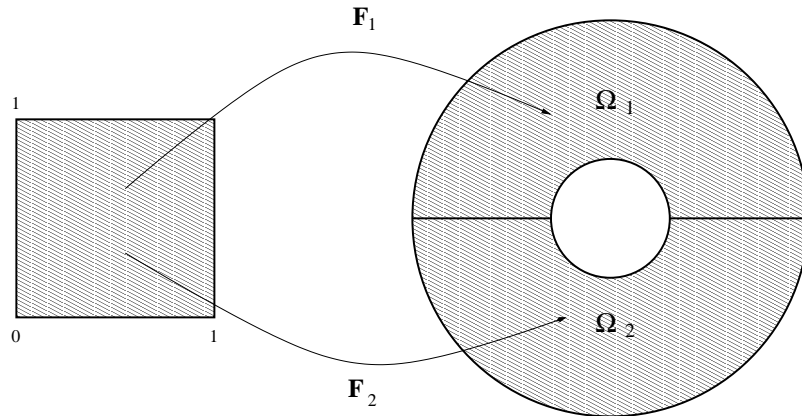


Fig. 3. Multiply connected  $\Omega$ , split into two simply connected domains  $\Omega_1$  and  $\Omega_2$ .

On each patch  $\Omega_\alpha$ , we define a space of potentials

$$\Phi_\alpha = \{\varphi \in H^2(\Omega_\alpha)/\mathbb{R}, \mathbf{curl} \varphi = \mathbf{0} \text{ on } \Gamma_D \cap \partial\Omega_\alpha\}, \quad (26)$$

whose curls give the space of divergence-free displacements on the patch:

$$\mathbf{K}_\alpha = \{\mathbf{v}|_{\Omega_\alpha}, \text{ with } \mathbf{v} \in \mathbf{K}\} \equiv \{\mathbf{curl} \varphi, \varphi \in \Phi_\alpha\}. \quad (27)$$

The space of *globally-defined* divergence-free displacements  $\mathbf{K}$ , defined in (3), can be obtained by glueing the  $\mathbf{K}_\alpha$ 's, i.e. by imposing continuity of the traces across the interior interfaces. More precisely, it holds

$$\mathbf{v} \in \mathbf{K} \Leftrightarrow \begin{cases} \mathbf{v}|_{\Omega_\alpha} \in \mathbf{K}_\alpha, & \forall \alpha = 1, \dots, N, \\ \mathbf{v}|_{\Omega_\alpha} = \mathbf{v}|_{\Omega_\beta} \text{ on } \partial\Omega_\alpha \cap \partial\Omega_\beta, & \forall \alpha, \beta = 1, \dots, N. \end{cases} \quad (28)$$

For the corresponding (patch-wise) potential  $\varphi$ , the glueing condition is therefore

$$\mathbf{curl} \varphi|_{\Omega_\alpha} = \mathbf{curl} \varphi|_{\Omega_\beta} \text{ on } \partial\Omega_\alpha \cap \partial\Omega_\beta, \forall \alpha, \beta = 1, \dots, N. \quad (29)$$

Hence, we here define the space  $\Phi$  as:

$$\Phi = \left\{ \varphi \in L^2(\Omega) : \varphi|_{\Omega_\alpha} \in \Phi_\alpha \ \alpha = 1, \dots, N ; \varphi \text{ fulfills Eqs (29)} \right\}. \quad (30)$$

**Remark 1** *The space  $\Phi$  defined in (30) is different from its analogous introduced in the single-patch approach (cf. (6)). Indeed, conditions (29) only imply that the jump of  $\varphi$  is constant across the interior interfaces, and, therefore,  $\varphi$  is not necessarily a continuous function. This is in accordance to what happens for multiply connected regions, where the existence of a globally continuous potential  $\varphi$  is not guaranteed, as it is well-known (see [12], for instance).*

Having introduced the space  $\Phi$ , the variational formulation of the problem on  $\Omega$  for the unknown  $\psi$  is still (7):

$$\left\{ \begin{array}{l} \text{Find } \psi \in \Phi \text{ such that} \\ 2\mu \int_{\Omega} \boldsymbol{\varepsilon}(\mathbf{curl} \psi) : \boldsymbol{\varepsilon}(\mathbf{curl} \varphi) = \int_{\Omega} \mathbf{f} \cdot \mathbf{curl} \varphi + \int_{\Gamma_N} \mathbf{g} \cdot \mathbf{curl} \varphi \end{array} \quad \forall \varphi \in \Phi, \right. \quad (31)$$

and the displacement is obtained as  $\mathbf{u} = \mathbf{curl} \psi$ .

At the discrete level, we are in a similar condition: on each patch  $\Omega_\alpha$ , a space of NURBS  $\Phi_{\alpha,h} \subset \Phi_\alpha$  is defined, as described in section 2. We then form the global approximation space

$$\Phi_h = \Phi_{1,h} \oplus \dots \oplus \Phi_{N,h} \equiv \left\{ \varphi_h \in L^2(\Omega) : \varphi_h|_{\Omega_\alpha} \in \Phi_{\alpha,h}, \ \alpha = 1, \dots, N \right\}.$$

Now, we could directly enforce the glueing conditions (29), by selecting  $\Phi_h \cap \Phi$  as discrete space. However, it is more convenient to work with a space  $\Phi_h \not\subset \Phi$ , employing a *Discontinuous Galerkin* technique (see [3], for example) to take conditions (29) into account. Similar Discontinuous Galerkin type techniques have been developed [7,8,13], for instance.

We show the basic idea on a very easy example, where a rectangular domain  $\Omega$  is split into two domains  $\Omega_1$  and  $\Omega_2$  sharing a common interface  $\Gamma$ , as depicted in Figure 4.

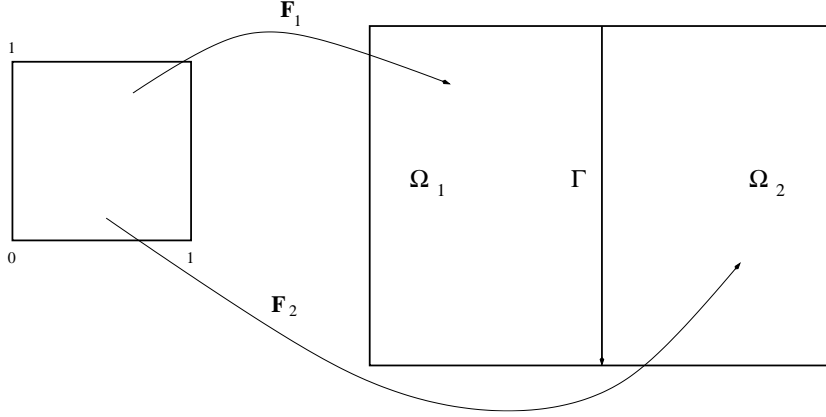


Fig. 4. Rectangular  $\Omega$ , split into two domains  $\Omega_1$  and  $\Omega_2$ .

The formulation we propose is the following.

$$\left\{ \begin{array}{l} \text{Find } \psi_h \in \Phi_h = \Phi_{1,h} \oplus \Phi_{2,h} \text{ such that} \\ 2\mu \sum_{\alpha=1}^2 \int_{\Omega_\alpha} \boldsymbol{\varepsilon}(\mathbf{curl} \psi_h) : \boldsymbol{\varepsilon}(\mathbf{curl} \varphi_h) - 2\mu \int_{\Gamma} \{ \{ \boldsymbol{\varepsilon}(\mathbf{curl} \psi_h) \} \} : \llbracket \mathbf{curl} \varphi_h \rrbracket \\ - 2\mu \int_{\Gamma} \llbracket \mathbf{curl} \psi_h \rrbracket : \{ \{ \boldsymbol{\varepsilon}(\mathbf{curl} \varphi_h) \} \} + 2\mu C_S \frac{p^2}{h} \int_{\Gamma} \llbracket \mathbf{curl} \psi_h \rrbracket : \llbracket \mathbf{curl} \varphi_h \rrbracket \\ = \int_{\Omega} \mathbf{f} \cdot \mathbf{curl} \varphi_h + \int_{\Gamma_N} \mathbf{g} \cdot \mathbf{curl} \varphi_h \quad \forall \varphi_h \in \Phi_h. \end{array} \right. \quad (32)$$

Here,  $\{ \{ \cdot \} \}$  and  $\llbracket \cdot \rrbracket$  denote the average and jump operators on the interface  $\Gamma$  (see [4], for example), while  $C_S$  is a dimensionless stabilizing constant. The three integrals on  $\Gamma$  deal with the non-conformity of  $\Phi_h$ , that is, with the lack of continuity of discrete displacements across the interface  $\Gamma$ .

**Remark 2** *We remark that formulation (32) is a strongly consistent discretization of problem (31), as typical for DG methods. A rigorous analysis of the NURBS schemes based on (32) can be developed by using the results of [6] in combination with the techniques of [7,8,13].*

## 4 Numerical tests

In this section we present some numerical experiments performed to show the capabilities of the numerical method previously introduced. For all tests, we select an incompressible material with  $\mu = 40$ . Moreover, we remark that here and in the following we express forces and lengths as  $KN$  and  $m$ , respectively.

### 4.1 Square block under a uniform body load with two constrained sides

We start considering a well-established problem taken from standard engineering literature. This test consists of a square block, subjected to a uniform body load  $\mathbf{f}$ , with two consecutive constrained sides (Figure 5), for which we set  $L = 1$  and  $\mathbf{f} = (0, -80)$ .

We then consider a reference solution obtained from the (locking-free) quadrilateral mixed-enhanced formulation proposed in [16], that we have coded within the research-oriented finite element code FEAP (see [19]). A very fine mesh of  $101 \times 101$  nodes (with two degrees of freedom per node) has been employed (see Figure 6). We check the solution in three points referred to as  $A$ ,  $B$  and  $C$ , whose coordinates are, respectively,  $(1/2, 1)$ ,  $(1, 1)$  and  $(1, 1/2)$  (cf. Figure 5). The reference solution in correspondence of  $A$ ,  $B$  and  $C$  is as follows:

- $\mathbf{u}_{ref}^A = (0.0782, -0.1575)$ ;
- $\mathbf{u}_{ref}^B = (0.0915, -0.1624)$ ;
- $\mathbf{u}_{ref}^C = (0.1658, -0.1176)$ .

In Figures 7 and 8 we report contour plots of the reference solution for the two displacement components over the deformed shape.

In Table 1, we report the solutions obtained with the method proposed in the present paper for different choices of approximation orders and grids, normalized with respect to the reference solutions (i.e., in terms of  $\tilde{u}_i = u_i / (u_{ref})_i$ ). In the last column of the table, we also report the number of degrees of freedom effectively employed for the computations.

We highlight that, in order to impose the boundary conditions, we have to prescribe zero displacements (i.e. zero gradient components for the stream function) on a part of the boundary (the left and the bottom side) that we indicate with  $\Gamma$ . To do that, we have just to impose zero values for all of the control points constituting  $\Gamma$  and for those adjacent to it, as in this way the stream function is forced to have zero normal and tangential derivative on  $\Gamma$ .

Moreover, in Figure 9, we report the control net and the mesh obtained using  $p = q = 4$  and  $31 \times 31$  control points, while in Figures 10–12 we report contour plots of the solution, obtained using such a mesh, in terms respectively of the stream function and of the displacement components. The latter are plotted over the deformed shape and they show the same behavior as in Figures 7 and 8.

As it is possible to observe from the numerical results, good solutions are obtained even using low-order NURBS interpolations over coarse grids.

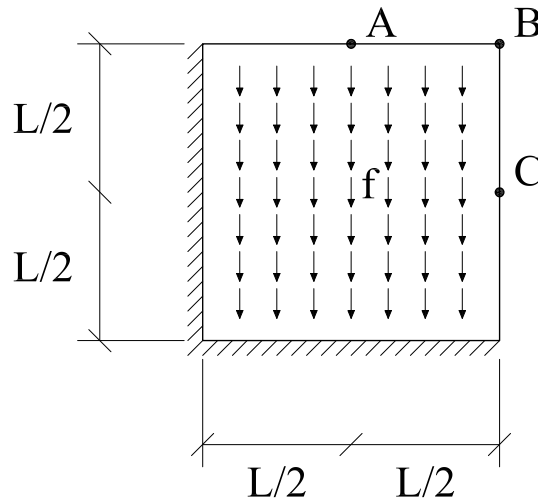


Fig. 5. Square block under a uniform body load with two constrained sides.

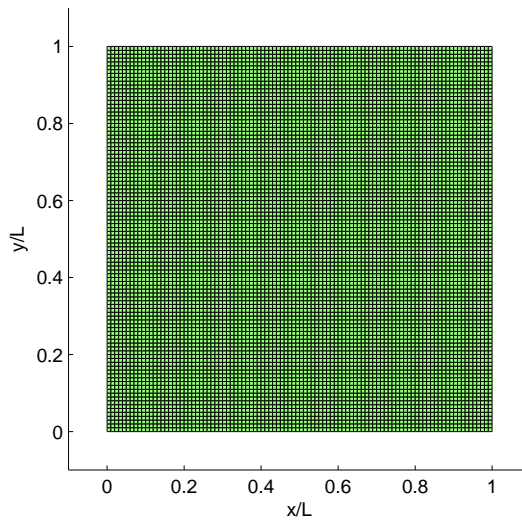


Fig. 6. Square block under a uniform body load with two constrained sides:  $101 \times 101$  node mesh employed to compute the reference solution. We recall that there are two degrees of freedom per node.

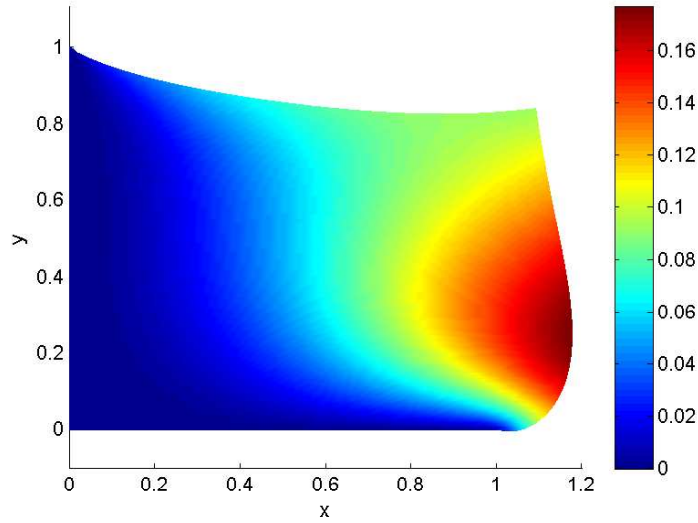


Fig. 7. Square block under a uniform body load with two constrained sides: reference solution for the first displacement component (over the deformed shape).

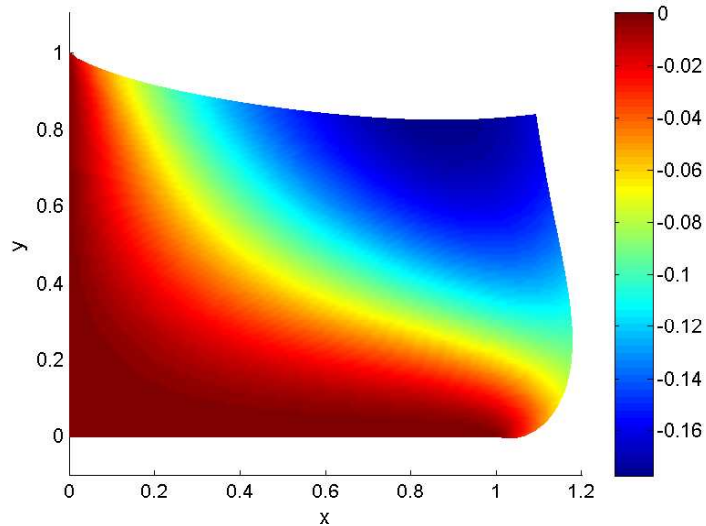


Fig. 8. Square block under a uniform body load with two constrained sides: reference solution for the second displacement component (over the deformed shape).

#### 4.2 Fully constrained square block with a trigonometric body load

The second test we consider consists of a fully constrained square block occupying the region  $\Omega = (-L, L) \times (-L, L)$ . We choose a particular body load  $\mathbf{f}$  for which the corresponding analytical solution  $\mathbf{u}$  is available (cf. [5]).

For this problem we set:

$$L = \pi/2,$$

order	c.p. grid	$\tilde{u}_x^A$	$\tilde{u}_y^A$	$\tilde{u}_x^B$	$\tilde{u}_y^B$	$\tilde{u}_x^C$	$\tilde{u}_y^C$	# of dofs
$2 \times 2$	$11 \times 11$	0.941	0.968	0.969	0.966	0.976	0.956	81
	$21 \times 21$	0.974	0.988	0.986	0.986	0.991	0.981	361
	$31 \times 31$	0.984	0.993	0.991	0.992	0.995	0.989	841
$3 \times 3$	$11 \times 11$	0.965	0.985	0.979	0.983	0.988	0.974	81
	$21 \times 21$	0.988	0.996	0.993	0.994	0.996	0.992	361
	$31 \times 31$	0.994	0.997	0.997	0.998	0.998	0.997	841
$4 \times 4$	$11 \times 11$	0.972	0.989	0.988	0.990	0.991	0.979	81
	$21 \times 21$	0.992	0.997	0.997	0.997	0.998	0.997	361
	$31 \times 31$	0.996	0.999	0.999	0.999	0.999	0.999	841

Table 1

Square block under a uniform body load with two constrained sides: normalized solutions at points  $A$ ,  $B$  and  $C$ .

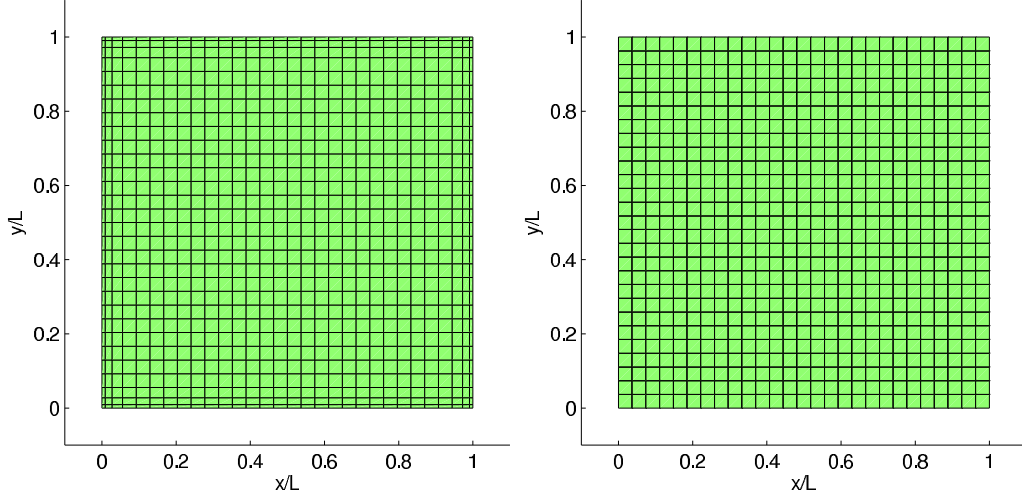


Fig. 9. Square block under a uniform body load with two constrained sides: control net and mesh obtained using  $p = q = 4$  and  $31 \times 31$  control points for the NURBS-based method. We recall that there is only one degree of freedom per control point.

$$f_1 = \mu \cos y \sin y (1 - 4 \cos^2 x) - 2xy \cos(x^2 y),$$

$$f_2 = -\mu \cos x \sin x (1 - 4 \cos^2 y) - x^2 \cos(x^2 y),$$

such that the analytical solution in terms of displacement components is:

$$u_1 = -\frac{\cos^2 x \cos y \sin y}{2},$$

$$u_2 = \frac{\cos^2 y \cos x \sin x}{2},$$

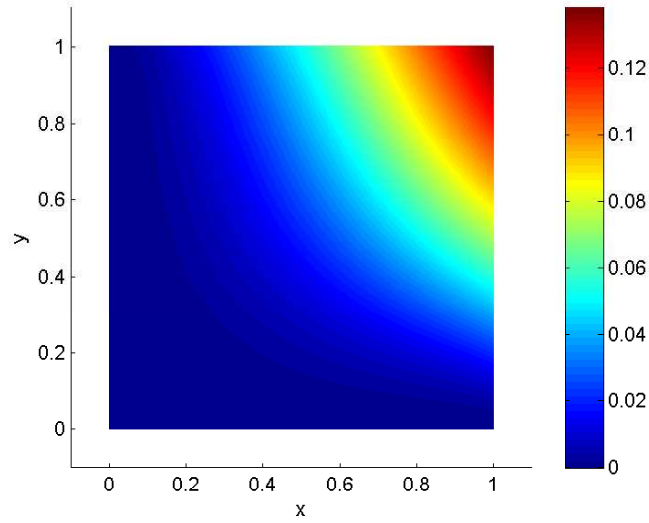


Fig. 10. Square block under a uniform body load with two constrained sides: stream function obtained using  $p = q = 4$  and  $31 \times 31$  control points.

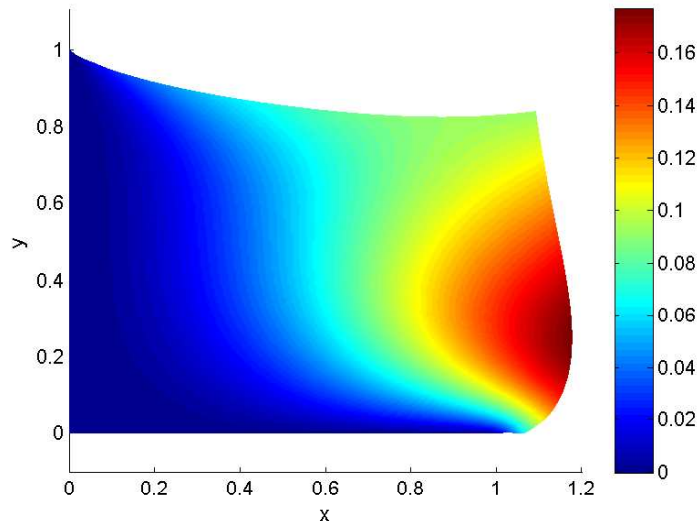


Fig. 11. Square block under a uniform body load with two constrained sides: first displacement component (over the deformed shape) obtained using  $p = q = 4$  and  $31 \times 31$  control points.

while the solution in terms of the stream function  $\psi$  reads as:

$$\psi = \frac{\cos^2 x \cos^2 y}{4}.$$

Analogously to the previous test, in Figures 13–15, we report contour plots of the solution, obtained using  $p = q = 4$  and  $31 \times 31$  control points, in terms of the stream function and of the displacement components. We remark that

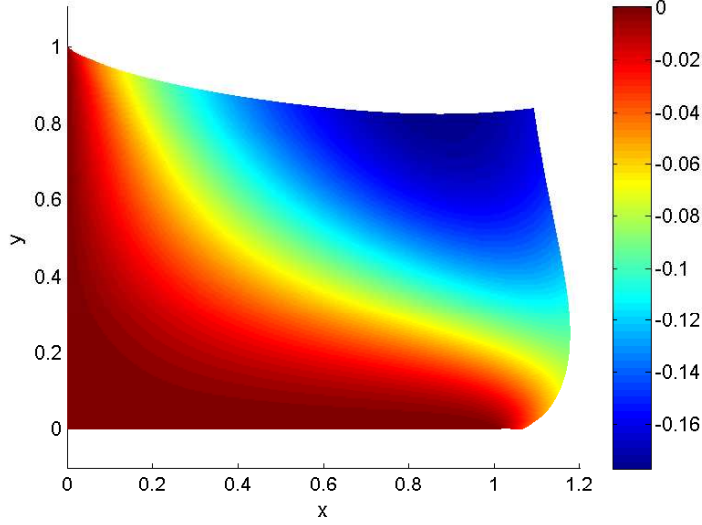


Fig. 12. Square block under a uniform body load with two constrained sides: second displacement component (over the deformed shape) obtained using  $p = q = 4$  and  $31 \times 31$  control points.

$p = q = 3$	-4.113	-3.702	-3.505	-3.394	-3.323	-3.274	-3.237	-3.210
$p = q = 4$	-6.286	-5.338	-4.942	-4.727	-4.592	-4.499	-4.432	-4.380

Table 2

Fully constrained square block with a trigonometric body load: slope sequence of the piece-wise linear curves in Figures 16 ( $p = q = 3$ ) and 17 ( $p = q = 4$ ).

in this case we have to impose zero displacement conditions on the whole boundary  $\partial\Omega$ ; this is obtained by prescribing the stream function to have zero values for all of the boundary control points and for those adjacent to  $\partial\Omega$ .

In Figures 16 and 17, we also report the convergence plots for the two components of the displacement field when using cubic and quartic approximations along each direction. We remark that, here and in the following, we compute errors using the  $L^2$ -norm (denoted by  $\|\cdot\|_0$ ). It is possible to observe (see also Table 2) that, even if for coarse grids we get higher rates of convergence than expected, such rates tend to the expected theoretical values (i.e., 3 and 4 respectively) as the grid gets finer and finer.

Moreover, in Figure 18, we study the convergence of the solution as a function of the order of approximation over a  $21 \times 21$  control point grid. As expected, an exponential rate of convergence with respect to the employed order is obtained.

Then, as we are interested in a comparison between the performance of the proposed approach with standard finite element techniques, in Figure 19 we show the convergence plots of Figures 16 and 17 as compared with the ones presented in [5,16] and obtained using some mixed-enhanced finite element

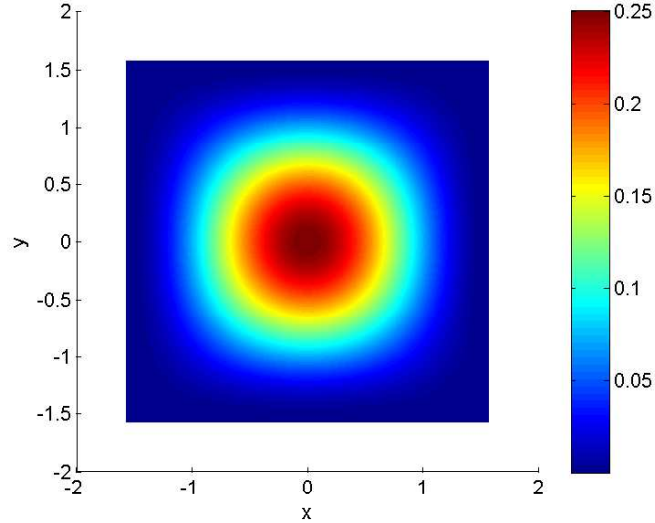


Fig. 13. Fully constrained square block with a trigonometric body load: stream function obtained using  $p = q = 4$  and  $31 \times 31$  control points.

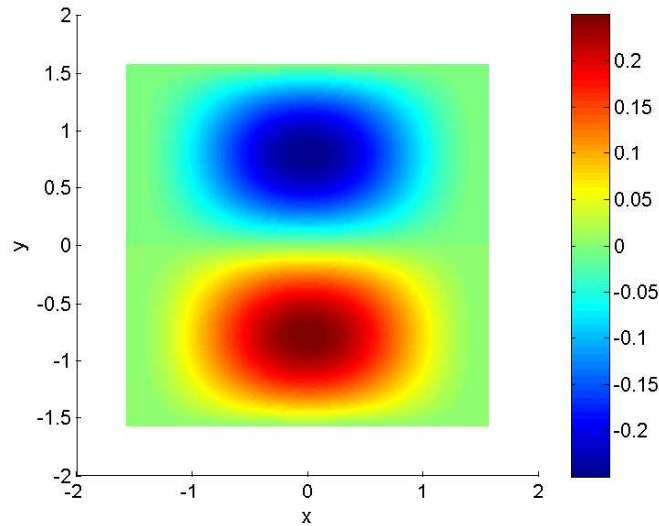


Fig. 14. Fully constrained square block with a trigonometric body load: first displacement component obtained using  $p = q = 4$  and  $31 \times 31$  control points.

formulations. The plots are in terms of relative  $L^2$ -norm errors of the displacement modulus, considered as a function of:

- (1) the number of control points per direction, for the NURBS discretizations of the stream function formulation;
- (2) the number of nodes per direction, for the finite elements discretizations essentially based on formulation (2).

It is worth noticing that:

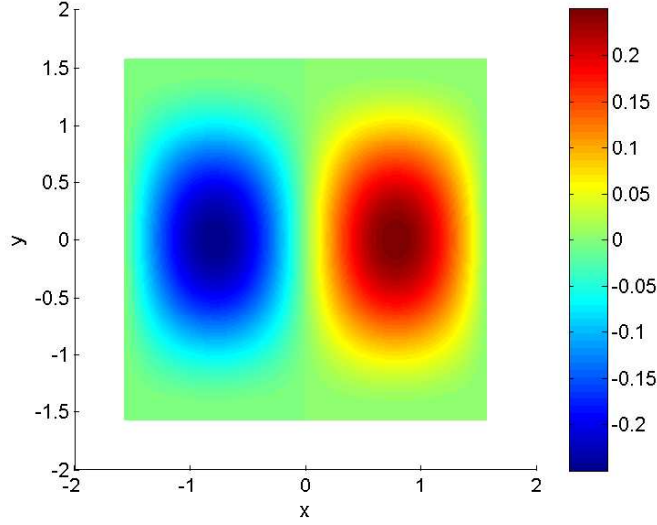


Fig. 15. Fully constrained square block with a trigonometric body load: second displacement component obtained using  $p = q = 4$  and  $31 \times 31$  control points.

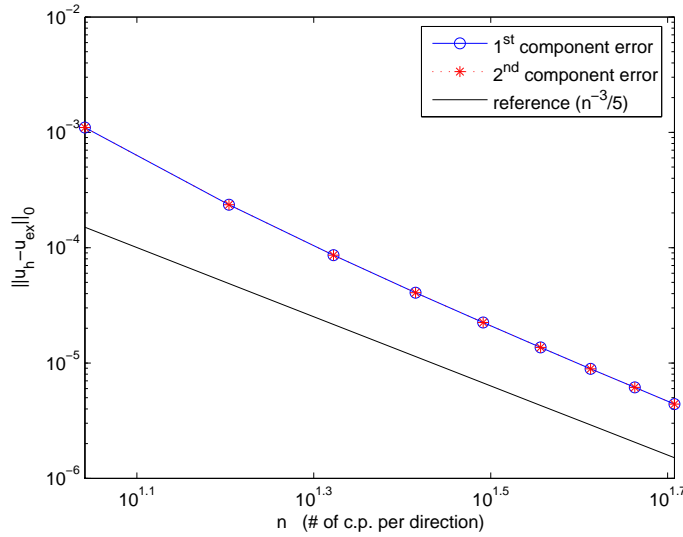


Fig. 16. Fully constrained square block with a trigonometric body load: solution convergence for  $p = q = 3$ .

- (1) control points in the adopted NURBS formulation and nodes in mixed-enhanced finite elements do not have an equal weight in terms of degrees of freedom, since for the new approach the unknown field is scalar. Namely, a control point corresponds to only one degree of freedom, while in the case of the mixed-enhanced finite elements each node corresponds to three degrees of freedom (two for the displacement components, one for the pressure).
- (2) The stiffness matrix corresponding to the NURBS approach is less sparse than the one arising from finite element procedures, due to the larger

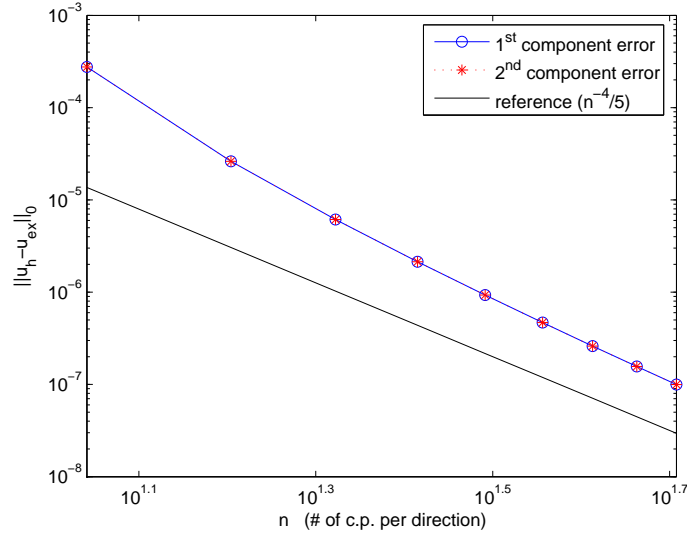


Fig. 17. Fully constrained square block with a trigonometric body load: solution convergence for  $p = q = 4$ .

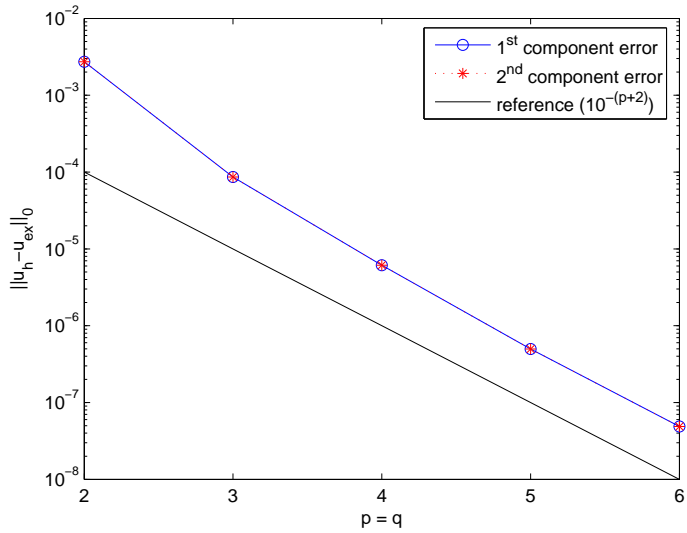


Fig. 18. Fully constrained square block with a trigonometric body load: solution convergence as a function of the order of approximation over a  $21 \times 21$  control point grid.

support of NURBS basis functions. In addition, a larger condition number is expected, as a result of the discretization of a fourth order problem.

We may reasonably assume that these two effects will even up in terms of computational costs. Therefore, we think that Figure 19 represents a *fair preliminary* comparison. Accordingly, the formulation proposed in this paper shows a superior behavior with respect to all the finite element approaches studied in [5].

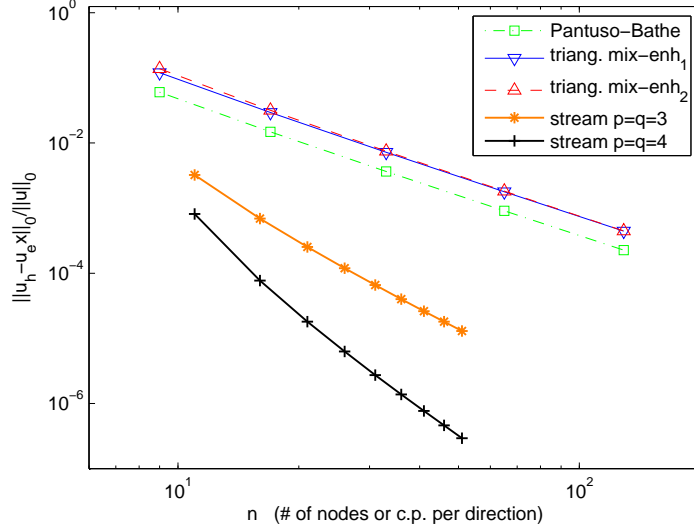


Fig. 19. Fully constrained square block with a trigonometric body load: solution convergence for different mixed-enhanced formulations (cf. [5,16], 3 d.o.f.’s per node) and for the proposed approach using cubic and quartic approximation (1 d.o.f. per control point).

We finally solve this example also using a multipatch approach, in order to test the formulation proposed in Section 3.2.

The problem consists of dividing the square domain  $\Omega = (-L, L) \times (-L, L)$  into two subdomains  $\Omega_1 = (-L, 0) \times (-L, L)$  and  $\Omega_2 = (0, L) \times (-L, L)$ , sharing the common interface  $\Gamma = \{0\} \times (-L, L)$  (cf. Figure 4). The formulation is then modified by the introduction of the integrals along  $\Gamma$ , as prescribed by (32), and choosing the stabilizing constant  $C_S = 10$ .

We conclude this example showing the convergence plots for cubic approximation (Figure 20), where it is shown that also for the multipatch solution the expected convergence rate is recovered.

#### 4.3 Fully constrained quarter of an annulus with a polynomial body load

As a last numerical experiment, we focus on the behavior of the method when studying a problem on a domain that cannot be represented exactly with standard finite elements. The selected domain  $\Omega$  is the quarter of an annulus reported in Figure 21, which is considered to be fully constrained along its boundary  $\partial\Omega$ . We remark that, again, boundary conditions are imposed by prescribing the stream function to have zero values for all of the boundary control points and for those adjacent to  $\partial\Omega$ .

Also for this example, we choose a particular body load  $\mathbf{f}$  for which the cor-

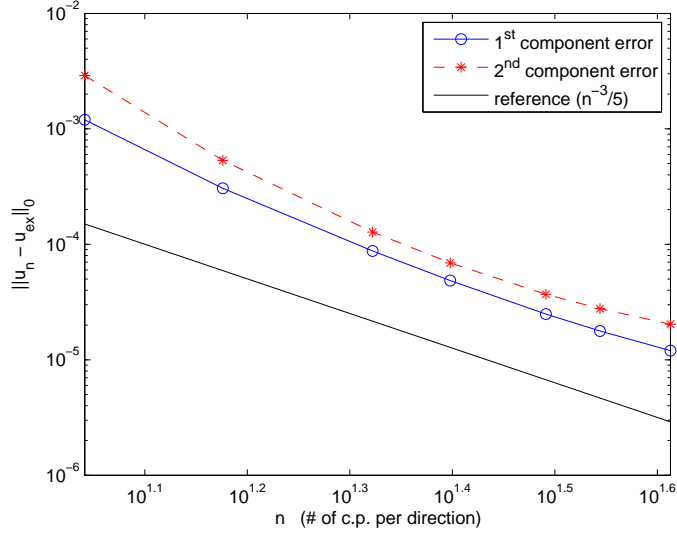


Fig. 20. Fully constrained square block with a trigonometric body load: solution convergence for  $p = q = 3$  for the two-patch case.

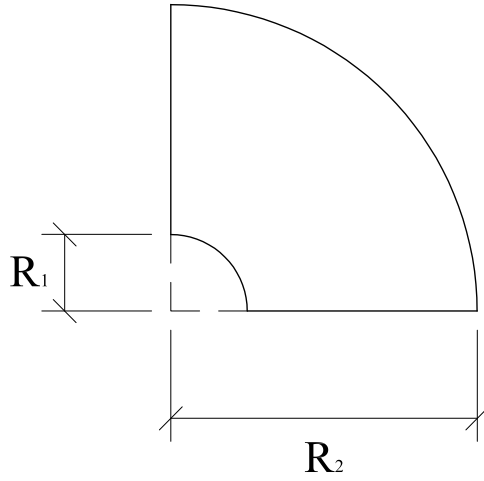


Fig. 21. Fully constrained quarter of an annulus with a polynomial body load: domain geometry.

responding analytical solution  $\mathbf{u}$  is available. We set:

$$R_1 = 1, R_2 = 4,$$

$$f_1 = -2 \cdot 10^{-6} y^2 \mu (91485x^4y^2 + 2296x^6y^4 + 2790x^4y^6 + 7680x^2 + 645x^8y^2 + \\ - 15470x^6y^2 - 3808y^4 + 2889y^6 + 1280y^2 - 36414x^4y^4 + 107856x^2y^4 + \\ + 13y^{10} - 374y^8 + 1122y^8x^2 - 22338y^6x^2 - 16320x^4 - 73440x^2y^2 + \\ + 9630x^6 - 1020x^8 + 30x^{10}),$$

$$f_2 = 8 \cdot 10^{-6} y^3 x \mu (7704y^4 + 1280 + 258x^6y^2 + 492x^4y^4 - 4641x^4y^2 + 310y^6x^2 + \\ - 5202x^2y^4 + 25x^8 - 680x^6 + 4815x^4 + 51y^8 - 1241y^6 + 18297x^2y^2 + \\ - 5440x^2 - 7344y^2),$$

such that the analytical solution in terms of displacement components is:

$$u_1 = 10^{-6} x^2 y^4 (x^2 + y^2 - 16)(x^2 + y^2 - 1)(5x^4 + 18x^2y^2 - 85x^2 + 13y^4 + 80 - 153y^2),$$

$$u_2 = -2 \cdot 10^{-6} x y^5 (x^2 + y^2 - 16)(x^2 + y^2 - 1)(5x^4 - 51x^2 + 6x^2y^2 - 17y^2 + 16 + y^4),$$

while the solution in terms of the stream function  $\psi$  reads as:

$$\psi = 10^{-6} (x^2 + y^2 - 1)^2 (x^2 + y^2 - 16)^2 x^2 y^5.$$

In Figure 22, we report the very coarse (but anyway capable of representing exact geometry) control net and mesh obtained using  $p = q = 2$  and  $4 \times 4$  control points along the two parametric directions, while in Figure 23 we report the ones obtained using  $p = q = 4$  and  $38 \times 36$  control points. We then show contour plots of the solution in terms of the stream function and of the displacement components over the finer mesh (Figures 24–26). Moreover, we report the convergence plots for the two components of the displacement field when using cubic ( $p = q = 3$ ) and quartic ( $p = q = 4$ ) approximations (Figures 27 and 28). Again, as shown by Table 3, the convergence rates tend to the expected values (i.e., 3 and 4 respectively) as the grid gets finer and finer.

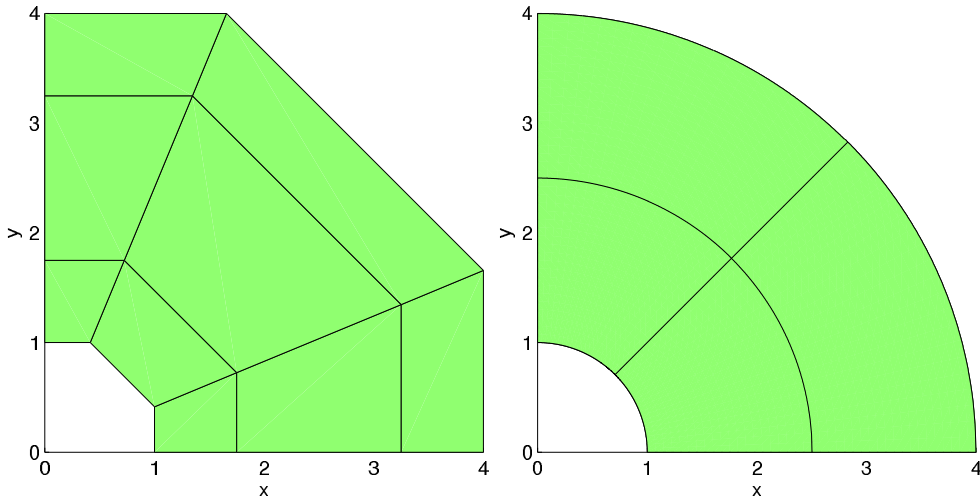


Fig. 22. Fully constrained quarter of an annulus with a polynomial body load: control net and mesh obtained using  $p = q = 2$  and  $4 \times 4$  control points.

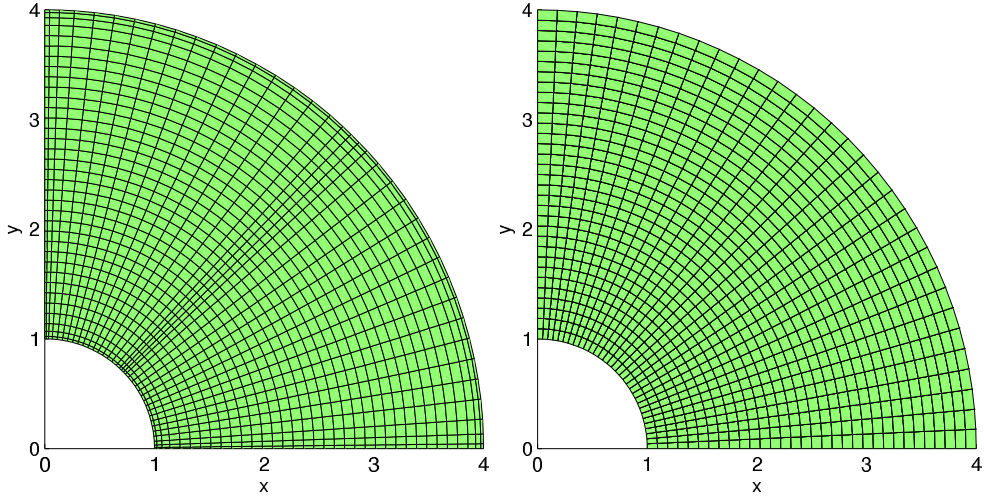


Fig. 23. Fully constrained quarter of an annulus with a polynomial body load: control net and mesh obtained using  $p = q = 4$  and  $38 \times 36$  control points.

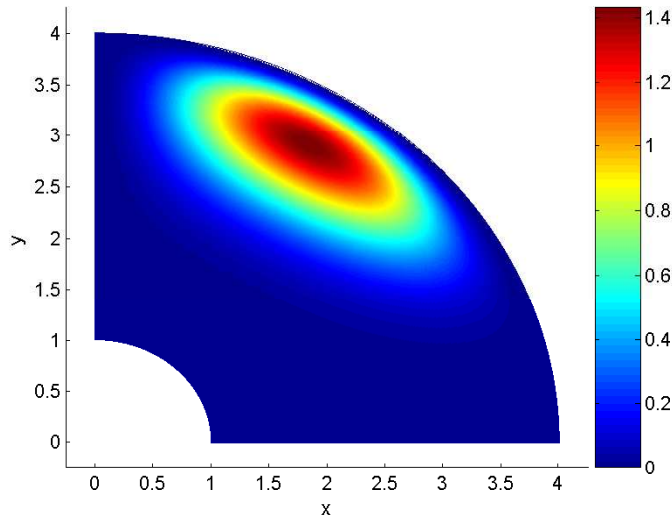


Fig. 24. Fully constrained quarter of an annulus with a polynomial body load: stream function obtained using  $p = q = 4$  and  $38 \times 36$  control points.

## Conclusions

We have presented an isogeometric analysis for plane linear incompressible elasticity problems. Our formulation stems from the introduction of a suitable *scalar potential function* which is able to easily describe the function space satisfying the incompressibility constraint. Several numerical experiments are provided to illustrate the actual performance of our approach, showing in particular the optimal convergence rates of the error.

We conclude by pointing out that, in our opinion, many extensions deserve

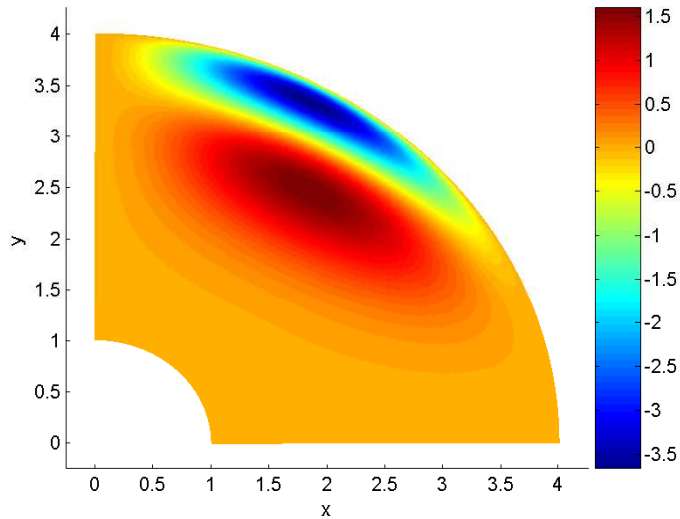


Fig. 25. Fully constrained quarter of an annulus with a polynomial body load: first displacement component obtained using  $p = q = 4$  and  $38 \times 36$  control points.

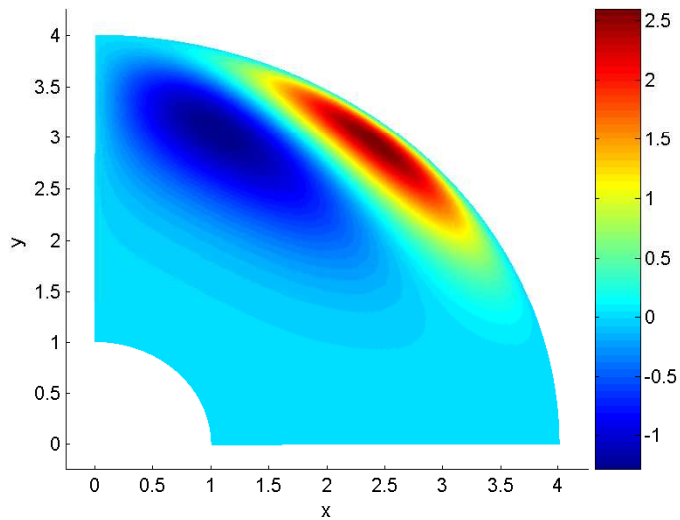


Fig. 26. Fully constrained quarter of an annulus with a polynomial body load: second displacement component obtained using  $p = q = 4$  and  $38 \times 36$  control points.

further investigations. Among them, we would like to mention the case of *nearly incompressible* materials, as well as the problem of designing efficient strategies for the *pressure recovery*. Furthermore, and more importantly, the *three-dimensional* elastic problem should be deeply considered. Such extensions, along with mathematical details on the formulation, will be the subject of future communications.

**Acknowledgments** The authors would like to thank Prof. T.J.R. Hughes,

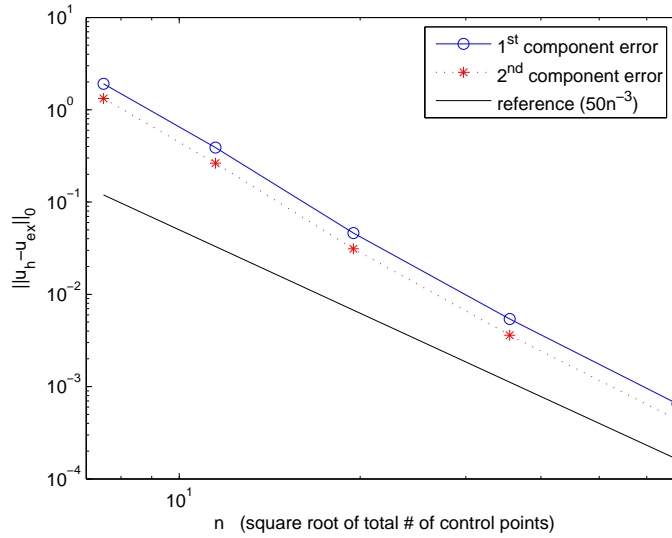


Fig. 27. Fully constrained quarter of an annulus with a polynomial body load: solution convergence for  $p = q = 3$ .

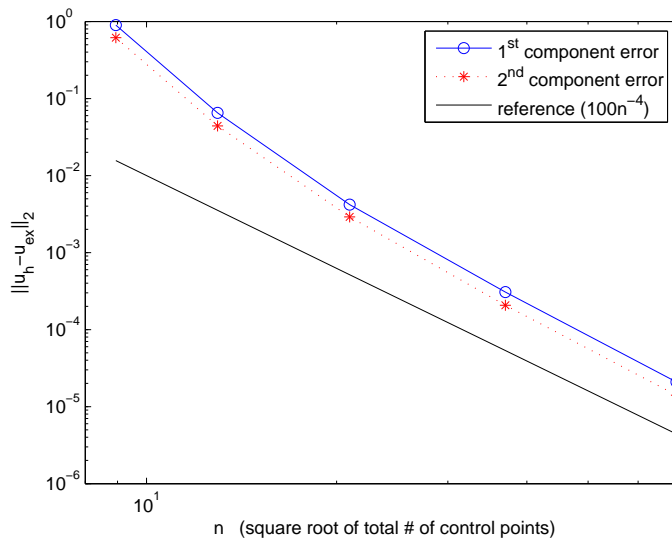


Fig. 28. Fully constrained quarter of an annulus with a polynomial body load: solution convergence for  $p = q = 4$ .

University of Texas at Austin, for the very valuable discussions on the subject of this paper.

## References

[1] C. Amrouche, C. Bernardi, M Dauge, and V. Girault. Vector potentials in three-dimensional non-smooth domains. *Math. Meth. Appl. Sci.*, 21:823–864,

$p = q = 3$ , 1 <sup>st</sup> component	-3.716	-4.030	-3.582	-3.297
$p = q = 3$ , 2 <sup>nd</sup> component	-3.766	-4.042	-3.603	-3.278
$p = q = 4$ , 1 <sup>st</sup> component	-7.068	-5.693	-4.614	-4.310
$p = q = 4$ , 2 <sup>nd</sup> component	-7.115	-5.654	-4.655	-4.310

Table 3

Fully constrained quarter of an annulus with a polynomial body load: slope sequence of the piece-wise linear curves in Figures 27 ( $p = q = 3$ ) and 28 ( $p = q = 4$ ).

1998.

- [2] J.H. Argyris, I. Fred, and D.W.Sharpf. The TUBA family of plate elements for the matrix displacement method. *Aero J. Royal Aeronaut. Soc.*, 72:701–709, 1968.
- [3] D.N. Arnold, F. Brezzi, B. Cockburn, and L.D. Marini. Unified analysis of discontinuous Galerkin methods for elliptic problems. *SIAM J. Numer. Anal.*, 39(5):1749–1779 (electronic), 2001/02.
- [4] D.N. Arnold, F. Brezzi, and L.D. Marini. A family of discontinuous Galerkin finite elements for the Reissner-Mindlin plate. *J. Sci. Comput.*, 22/23:25–45, 2005.
- [5] F. Auricchio, L. Beirão da Veiga, C. Lovadina, and A. Reali. An analysis of some mixed-enhanced finite element for plane linear elasticity. *Comput. Methods Appl. Mech. Engrg.*, 5:2947–2968, 2005.
- [6] Y. Bazilevs, L. Beirão da Veiga, J.A. Cottrell, T.J.R. Hughes, and G. Sangalli. Isogeometric analysis: approximation, stability and error estimates for  $h$ -refined meshes. *Math. Models Methods Appl. Sci.*, 16(7):1031–1090, 2006.
- [7] S. Brenner, F. Li, and L.Y. Sung. A locally divergence-free nonconforming finite element method for the time harmonic Maxwell equations. *Math. of Comp.*, 76:573–595, 2007.
- [8] S. Brenner and L.Y. Sung.  $C^0$  interior penalty methods for fourth order elliptic boundary value problems on polygonal domains. *J. Sci. Comput.*, 22/23:83–118, 2005.
- [9] F. Brezzi and M. Fortin. *Mixed and Hybrid Finite Element Methods*. Springer-Verlag, Berlin, 1991.
- [10] J.A. Cottrell, A. Reali, Y. Bazilevs, and T.J.R. Hughes. Isogeometric analysis of structural vibrations. *Comput. Methods Appl. Mech. Engrg.*, 195(41-43):5257–5296, 2006.
- [11] G.E. Farin. *NURBS curves and surfaces: from projective geometry to practical use*. A. K. Peters, Ltd., Natick, MA, 1995.
- [12] V. Girault and P.-A. Raviart. *Finite element approximation of the Navier-Stokes equations*. Springer-Verlag, Berlin-New York, 1979.

- [13] P. Hansbo and M.G. Larson. Piecewise Divergence Free Discontinuous Galerkin Methods for Stokes Flow. *Communications in Numerical Methods in Engineering*, to appear.
- [14] T. J. R. Hughes. *The Finite Element Method: Linear Static and Dynamic Finite Element Analysis*. Dover Publications, Mineola, New York, 2000.
- [15] T.J.R. Hughes, J.A. Cottrell, and Y. Bazilevs. Isogeometric analysis: CAD, finite elements, NURBS, exact geometry, and mesh refinement. *Computer Methods in Applied Mechanics and Engineering*, 194:4135–4195, 2005.
- [16] D. Pantuso and K.-J. Bathe. A four-node quadrilateral mixed-interpolated element for solids and fluids. *Math. Models Methods Appl. Sci.*, 5:1113–1128, 1995.
- [17] L. Piegl and W. Tiller. *The NURBS Book (Monographs in Visual Communication)*, 2nd ed. Springer-Verlag, New York, 1997.
- [18] D. F. Rogers. *An Introduction to NURBS With Historical Perspective*. Academic Press, San Diego, CA, 2001.
- [19] R. L. Taylor. FEAP: A Finite Element Analysis Program, programmer manual. <http://www.ce.berkeley.edu/~rlt/feap/>, 2001.
- [20] S. Timoshenko and J.N. Goodier. *Theory of Elasticity, Second Edition*. McGraw-Hill, New York, 1951.
- [21] O. C. Zienkiewicz and R. L. Taylor. *The finite element method. Vol. 1*. Butterworth-Heinemann, Oxford, fifth edition, 2000. The basis.